JOURNAL OF SOLID STATE CHEMISTRY 115, 490–498 (1995)

Relations between Oxygen Deficiency and Structures in the La–Sr–Cu–O System

III. Oxygen Content and Structure of the $(La,Sr)_8Cu_8O_{16+\delta}$ Phase

Kenji Otzschi, Keiichi Koga, and Yutaka Ueda

Institute for Solid State Physics, University of Tokyo, 7-22-1 Roppongi, Minato-ku, Tokyo 106, Japan

Received December 31, 1993; in revised form June 20, 1994; accepted June 23, 1994

The 8-8-16 + δ phase ($(La_{1-x}Sr_x)_8Cu_8O_{16+\delta}$; x = 0.70 to 0.80) was investigated precisely. The oxygen content increases with increasing partial pressure of oxygen, for example, x = 0.75; δ = 0.08 (annealed under Ar at 810°C), δ = 0.27 (quenched from 1050°C in air; as-prepared), δ = 2.29 (annealed in O_2 at 800°C), and δ = 2.54 (treated under O_2 at high pressure (300 atm)). X-ray diffraction study, however, disclosed that there are two distinct phases, an oxygen-poor phase ($\delta \approx 0.0$: the 8-8-16 phase) and an oxygen-rich phase ($\delta \geq 2.0$: the 8-8-18 phase); as-prepared samples were a mixture of these two phases. These results disagree with those in the literature: δ = 0.0 for as-prepared and δ = 1.6 for O_2-annealed. Structural refinements for the 8-8-16 and the 8-8-18 phases were carried out with x = 0.775 samples by the powder X-ray Rietveld method. They revealed oxygen insertion into the interstitial positions on the basal "Cu–O plane" in the 8-8-18 phase. Electrical resistivity data show semiconductor-like (8-8-16 phase) or metallic (8-8-18 phase) behavior. The weak temperature dependence of their magnetic susceptibility can be substantially explained by Pauli paramagnetism.

1. INTRODUCTION

The La–Sr–Cu–O system has been extensively investigated during the past decade since it includes some superconducting phases as well as the La–Ba–Cu–O and the Y–Ba–Cu–O systems. Actually, two phases in the La–Sr–Cu–O system, $(La_{1-x}Sr_x)_2CuO_{4+\delta}$, (the so-called 2-1-4 phase, 1) and $SrCuO_2$ (2, 3), have been known to show superconducting behavior. The former contains a single CuO_2 layer in the structure and strontium doping or oxygen nonstoichiometry lead to a superconductor with $T_c \approx 40$ K (4, 5), where extra oxygen atoms are known to be inserted into the interstitial positions between La–O layers. The latter, which we call the 1-1-2 phase, crystallizes in an orthorhombic unit cell under ambient conditions (6) and shows a structural phase transition to the infinite layer structure under high pressure and high temperature. The latter form contains infinite CuO_2 planes isolated by Sr layers and shows superconductivity because of defects in the Sr- or CuO_2 layers.

Before and during these studies on superconducting objects, some other metallic or semiconducting but not superconducting compounds have been found and characterized by Raveau and co-workers (7, 8), De Leeuw *et al.* (4), and Fu *et al.* (9) in this system. Those are $(La_{1-x}Sr_x)_3Cu_2O_6$ (x = 0.3333 to 0.38; the 3-2-6 phase), $(La_{1-x}Sr_x)_3Cu_2O_{5.5+\delta}$ (x = 0.62 to 0.65; δ = 0.3 for x = 0.6333; the 3-2-5.5 phase), $(La_{1-x}Sr_x)_8Cu_8O_{20}$ (x = 0.16 to 0.24; the 8-8-20 phase) and $(La_{1-x}Sr_x)_8Cu_8O_{16+\delta}$ (x = 0.75; δ = 0.0 and 1.6; the 8-8-16 + δ phase). The structures of these cuprates are closely related to that of perovskite, where the ordering of oxygen vacancies and various oxygen coordinations around copper are the characteristics. The 3-2-6 phase, which is usually called the 2126 phase, has a two-dimensional structure containing CuO_2 planes as a result of peculiar omitting of oxygen atoms around Sr(La), and shows oxygen nonstoichiometry according to these oxygen atoms. The 3-2-5.5 phase was first found for Sm, Eu, and Gd by Nguyen *et al.* (10), and recently for La (4), and its structure is essentially based on that of the 3-2-6 phase; oxygen vacancies, however, are distributed in the CuO_2 planes as well.

In comparison to these two phases on the (La + Sr): Cu = 3:2 line, the other two phases on the (La + Sr): Cu = 1:1 line, which we call the "perovskite line," the 8-8-20 and 8-8-16 + δ phase have more three-dimensionally characterized structures owing to the considerable distribution of oxygen vacancies on the basal CuO_2 plane (8, 11, 12). La and Sr atoms in these phases are statistically distributed because of the similarity of the ionic radii of these two cations (13). Oxygen content of the 8-8-20 phase is unchangeable with both strontium concentration x and temperature; annealing it under oxygen at high pressure does not result in the insertion of extra oxygen atoms into the vacancies but results in the structural transition into the 5-5-13 phase ($(La_{1-x}Sr_x)_5Cu_5O_{13}$, x = 0.1666, 13) with

0022-4596/95 $6.00

an increase in oxygen content. Recently another oxygen deficient phase $(La_{1-x}Sr_x)_4Cu_4O_{10}$ (x = 0.135 to 0.15; the 4-4-10 phase) was found (14) to be the low-temperature form of the 8-8-20 phase and to have a different manner of oxygen-vacancy ordering in spite of the same metal–oxygen ratio. The 8-8-16 + δ phase was first found by Fu *et al.* (9) as an oxygen-deficient perovskite, where δ is 0.02 for the air-quenched sample and 1.56 for the air-annealed sample, and their unit-cell size is almost the same as that of the 8-8-20 phase. Structural refinements were first carried out by Fujishita *et al.* (15) using X-ray diffraction patterns in the space group $P42_12$ and $P42_1m$. Recent reports by Fu *et al.* (11, 12) on these structures using electron and neutron diffraction, however, contradict Fujishita's results and require that the space group is $P4/mbm$ for both δ = 0.02 and 1.56.

As mentioned above, we studied the phases on the perovskite line and recently discovered two new phases, the 5-5-13 phase and the 4-4-10 phase. Besides these investigations on the Sr-poor region, we are now researching the Sr-rich compound 8-8-16 + δ. We obtained, however, somewhat different results from these reported in the literature. The oxygen contents (x = 0.75) were δ = 0.27 and 2.29 for liquid N_2-quenched and O_2-annealed, respectively. In this brief report, we describe the reason for this discrepancy and describe their refined structures using X-ray diffraction patterns and show the relations between oxygen deficiency and structures. The changes in electrical and magnetic properties with various strontium concentrations and oxygen contents are also reported.

2. EXPERIMENTAL

All samples were prepared by solid state reaction in an alumina crucible covered with platinum foil from appropriate mixtures of predried La_2O_3, $SrCO_3$, and CuO in a ratio of $(1 - x)/2 : x : 1$ (x = 0.70, 0.725, 0.75, 0.775, 0.80). Heat treatments were carried out mainly according to the method of Fu *et al.* (9). The mixtures were first decarbonated in air at 900–950°C for several hours. Then the powders were reground, pressed into pellets, sintered in air at 1050°C for 3 hr, and quickly quenched in liquid N_2. This procedure was repeated once more in order to obtain a more homogeneous phase (as-prepared). The quenching or cooling conditions (mainly cooling rate and atmosphere) influence the oxygen content and the phase homogeneity (15); we also tried other kinds of cooling methods (see Results for details).

The as-prepared samples were then annealed in the three kinds of atmosphere: Ar, O_2, and O_2 high-pressure. Annealing in flowing Ar gas (purity >99.9999%) was performed at 810°C for 10 hr and the samples were cooled to room temperature as quickly as possible (in about 30 min; Ar-annealed). Annealing in flowing O_2 gas (>99.9995%) was carried out at 800°C for 2 hr; then the samples were very slowly cooled (30°C/hr) to room temperature in the furnace (O_2-annealed). The high-pressure treatment was performed in a non-isostatic manner. The gold tubes containing the samples were put into the high-pressure vessel, and the high-pressured oxygen gas (120–140 atm) was let into it. Then the vessel was put into the furnace and heated to 600°C in 1.5 hr. The pressure rose over 300 atm during the heating. This condition was kept for 2–3 hr. Then vessel was cooled quickly by taking it out of the furnace (O_2-high pressure).

Powder X-ray diffraction patterns were collected using a Mac Science MXP[18] system with a rotating anode generator and a monochromator of single crystalline graphite for $CuK\alpha$ radiation with a step of 0.02°. Rietveld refinement was made by the analysis program RIETAN (16) using the XRD profiles in the range 2θ = 10 to 106° for Ar-annealed and 18 to 114° for O_2-annealed and O_2-high-pressured. Some regions showing small peaks which could be assigned to the known impurities were excluded in the calculation (see Results).

The oxygen contents and nonstoichiometry were obtained by thermogravimetric and differential thermal analysis using a Mac Science TG-DTA 2000 assembly under various atmospheres. The weight loss by heating in the diluted hydrogen gas (10% H_2/He) to 900 to 950°C (15°C/min) gives the composition of oxygen assuming that the compound is finally decomposed and reduced into a mixture of Cu-metal, SrO, and La_2O_3. Other conditions of the heat treatments are described in Results.

Electrical resistivity measurements were carried out by the four probe method in the range 5 to 280 K at 1 K intervals. Magnetic susceptibility was measured by the conventional Faraday method with H_{ext} = 11.8 kOe in the temperature range 4.2 to 300 K.

3. RESULTS AND DISCUSSION

Phase Relations and Oxygen Contents

As already reported in the published literature (4), at 950°C under 1 bar of oxygen those regions around x = 0.75 in the formula $(La_{1-x}Sr_x)CuO_y$ are triphasic with the 1-1-2 phase, the 3-2-6 phase, and with $(La_{1-x}Sr_x)_{14}Cu_{24}O_{41}$ (the 14-24-41 phase (17, 18)). The 8-8-16 + δ phase is synthesized at higher temperature (1050°C) in a more reductive atmosphere (air). Reheating at 1025°C in O_2 resulted in the decomposition into the three phases cited above. In the literature, the oxygen content was reported to be δ = 0.02 for the air-quenched sample (the 8-8-16 phase), and δ = 1.56 for the air-annealed sample (for the 8-8-18 phase, see below). It was also described that the air-quenched sample contains the 8-8-18 phase as a little impurity. Therefore we adopted quick quenching in liquid N_2 as the cooling method in order to minimize the contami-

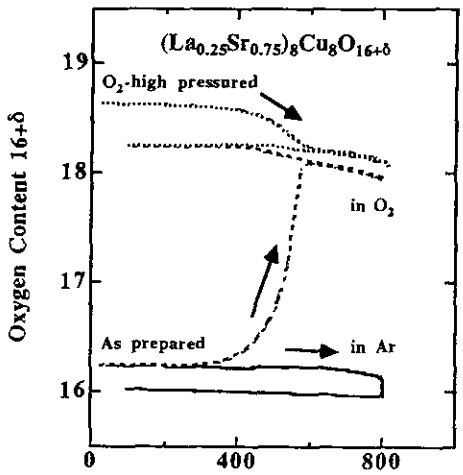

FIG. 1. The changes of the oxygen content of the as-prepared $(La_{0.25}Sr_{0.75})_8Cu_8O_{16.27}$ in Ar (solid line) and O_2 (dashed line), and the O_2-high pressured $(La_{0.25}Sr_{0.75})_8Cu_8O_{18.54}$ in O_2 (dots). Heating and cooling rates were at 10°C/min for Ar-annealing and 10°C–1°C/min for O_2-annealing; temperature was kept at 810°C for 10 hr and at 800°C for 2 hr, respectively.

nating low-temperature phases and to avoid oxygen contact. We obtained, however, the oxygen content $\delta = 0.27$ ($x = 0.75$) for the as-prepared sample, which is much larger than the value of 0.02 reported in the literature. The samples cooled more slowly to room temperature showed far larger oxygen contents; $\delta = 0.64$ for the air-quenched on a cool alumina boat and $\delta = 1.44$ for the air-cooled with a hot alumina boat. The larger the oxygen content, the greater was the amount of the 8-8-18 impurity.

Because the 8-8-18 phase can be considered to be the oxygenated form of the 8-8-16 phase (12), we tried the thermogravimetric analysis (TGA) of the as-prepared sample ($x = 0.75$) in pure Ar atmosphere and obtained the weight-loss curve with a heating rate of 10°C/min at constant temperature of 810°C for 10 hr. The results are shown in Fig. 1. The weight decrease began around 650°C and was completed after holding the temperature at 810°C for about 3 hr. We obtained the oxygen content $\delta = 0.08$ for this Ar-annealed sample and no contamination by the 8-8-18 phase was observed by powder XRD. Such a reductive atmosphere (Ar) is necessary in order to obtain the pure 8-8-16 phase described above and we think that the reported oxygen content $\delta = 0.02$ (9) for the air-quenched was due to the misestimation of its authors.

Figure 1 also shows the weight increase of the as-prepared sample in O_2. The heating and cooling rate were 10°C/min and 1°C/min, respectively, and temperature was held at 800°C for 2 hr (O_2-annealed). The sample begins to capture oxygen at around 400°C, and the weight increases to $\delta = 2.10$ by 600°C and then slightly decreases to $\delta = 1.99$ up to 800°C. Finally, the oxygen content comes to $\delta = 2.29$ after slowly cooling to room temperature. This TG curve is consistent with a structural transition of the 8-8-16 phase into the 8-8-18 phase. The obtained oxygen content $\delta = 2.29$ also disagrees with the literature value of 1.56. We think this is also due to the misestimation of its authors. Moreover, the difference between the oxygen content of the as-prepared sample and that of the O_2-annealed sample ($\Delta\delta$) is important; $\Delta\delta = 1.54$ ($= 1.56–0.02$) in the literature and $\Delta\delta = 1.65$ ($= 2.29–0.64$) for our results. This similarity between their and our $\Delta\delta$ values suggests that their misestimation of the oxygen content of the as-prepared sample resulted in misestimation again for the O_2-annealed sample.

The more oxygenated sample (O_2-high pressure) with $x = 0.75$ gave the oxygen content of 18.54, and the XRD pattern for this sample was very similar to that of the O_2-annealed. These observations mean that the structural phase transition is not induced by high oxygen pressure and that extra oxygen atoms are randomly inserted into the structure; no additional superstructures were observed. The 8-8-18 phase shows oxygen nonstoichiometry, which is in contrast to the phase transition of the 8-8-20 and 4-4-10 phases into the 5-5-13 phase by the same condition (13). These extra oxygen atoms are released at 400–600°C (Fig. 1, dots), and the composition of the sample becomes $\delta = 2.29$.

Our observations above revealed two distinct phases, the 8-8-16 phase ($\delta \approx 0.0$) and the 8-8-18 phase ($\delta \geq 2.0$), and the samples with $0 < \delta < 2.0$ are the mixture of these two phases. The 8-8-18 phase thus shows oxygen nonstoichiometry in the oxygen-rich side. TG analysis of the 8-8-18 phase in O_2 showed a reversible weight change, that is oxygen loss and gain, with a step of around $\delta \approx 2.05$ to 2.10 at 550°C. Of course, under Ar atmosphere, the 8-8-18 phase lost weight to produce $\delta \approx 0.0$.

The TG curve of the 8-8-18 phases at higher temperature was reported for the air-annealed sample "$(La_{0.25}Sr_{0.75})_8Cu_8O_{17.6}$" (9), which shows a weight decrease to "$(La_{0.25}Sr_{0.75})_8Cu_8O_{16.0}$" at 900°C. As already stated above, the O_2-annealed sample has a formula $(La_{0.25}Sr_{0.75})_8Cu_8O_{18.29}$, and so the profile given in the literature is considered to be curve shifted -0.6 to -0.7 in the δ-direction. Figure 2 shows the weight change of $(La_{0.25}Sr_{0.75})_8Cu_8O_{18.29}$ in air (solid line) and in O_2 (dashed line) with a heating/cooling rate 10°C/min. Each line shows a step of around $\delta \approx 2.10$ at 620 to 650°C as described above, which is not clear in the literature, and a rapid decrease from 800°C. The minimum values are $\delta = 0.51$ (in air, at 1025°C) and $\delta = 0.72$ (in O_2, at 985°C). The upturn in O_2 can be assigned to decomposition into the 3-2-6, 1-1-2, and 14-24-41 phases and indicates instability of Cu(I) in the 8-8-16 phase. Actually this upturn was not clearly observed in the more reductive atmosphere, air. The change of the oxygen content is $\Delta\delta = 1.78$ (in

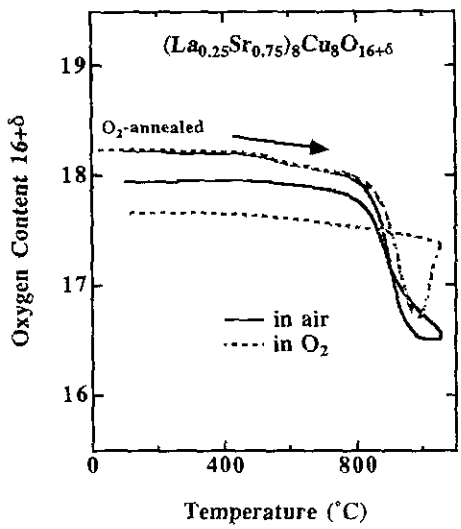

FIG. 2. The changes of the oxygen content of the O_2-annealed $(La_{0.25}Sr_{0.75})_8Cu_8O_{18.29}$ in air (solid line) and in O_2 (dashed line). The sample was heated and cooled at a rate of 10°C/min.

air) and 1.57 (in O_2), and these values are close to that in the literature (1.6). This similarity indicates that both we and Fu *et al.* use the same air- or O_2-annealed sample. In our opinion, however, the oxygen content never reaches $\delta = 0.0$ in air.

Oxygen contents of the 8-8-16 and 8-8-18 phases with both heat treatments and strontium concentration are summarized in Fig. 3. The strontium-poor ($x \approx 0.7$) and strontium-rich ($x \approx 0.8$) samples were contaminated by the low-temperature phases, the 3-2-6 phase and the 1-1-2 phase (and the 14-24-41 phase) respectively, which were observed by XRD as very small peaks but ignored in the following discussion. This diagram shows the great

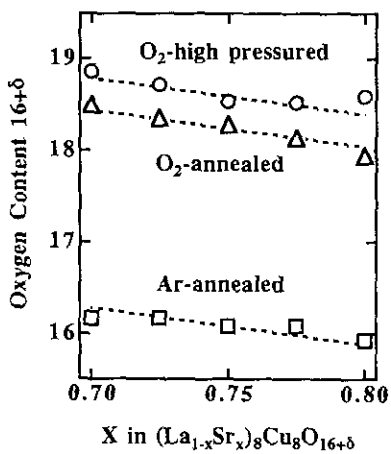

FIG. 3. Oxygen contents vs strontium concentration in $(La_{1-x}Sr_x)_8Cu_8O_{16+\delta}$: Ar-annealed (squares), O_2-annealed (triangles), and O_2-high pressure (circles). Dotted lines show the linear fit.

change of oxygen contents from the 8-8-16 phase ($\delta \approx 0.0$) to the 8-8-18 phase ($\delta \geq 2.0$), which is in contrast to the narrow oxygen-nonstoichiometry ranges of the other oxygen-deficient phases, the 8-8-20 and 4-4-10 phases (14). This difference can be considered to come from the oxygen deficiency. The 8-8-20 and 8-8-16 + δ have the similar sized unit cell $\approx 2\sqrt{2}a_p \times 2\sqrt{2}a_p \times a_p$ and the 4-4-10 has half its size, where a_p is the lattice parameter of an ideal cubic perovskite. The amounts of oxygen vacancies, however, are very different among these phases: 16.7% for the 8-8-20 and 4-4-10 phases and 33% for the 8-8-16 phase, where (La, Sr)CuO_3 is assumed to be the completely packed formula. Additional oxygen atoms can be inserted more easily into the 8-8-16 structure than the 8-8-20 or 4-4-10 one because of the larger oxygen deficiency of the former.

Besides being variable owing to heat treatments, the oxygen contents also depend on the amount of strontium, that is, the larger the strontium concentration, the smaller is the amount of oxygen. This behavior of oxygen nonstoichiometry in the 8-8-16 and 8-8-18 phases can be due to charge compensation for strontium doping. The oxygen content of each sample can be roughly calculated by the linear fit; $\delta = 3.08 - 4x$ (Ar-annealed), $5.24 - 4x$ (O_2-annealed) and $5.60 - 4x$ (O_2-high pressure). Conversely, by assuming that the respective oxidation numbers of La, Sr, and O are +3, +2, and −2, the oxidation number of copper can be calculated as 1.77 for Ar-annealed, 2.31 for O_2-annealed, and 2.40 for O_2-high pressured, although the O_2-high pressured with $x = 0.80$ exhibits a large deviation of 2.45. These behaviors are quite different from those of the 8-8-20 and 4-4-10 phases, where the formal oxidation state of Cu, rather than the oxygen content, changes with strontium concentration. The change in oxygen content for the sake of charge compensation can also be accommodated by the high oxygen deficiency of this phase relative to the other perovskites.

Rietveld Refinement and Structural Properties

The refined structure of the 8-8-16 + δ ($\delta = 0.0$, 1.6) phases have already been described in several published reports (11, 12, 15), but there are some faults in them, including incorrect space group, misestimation of oxygen contents, and coexistence of oxygen-poor and -rich phases. Therefore we show our refinement results using reliable samples.

Figure 4 shows the lattice constants of the samples, $x = 0.70$ to 0.8, Ar-annealed, O_2-annealed, and O_2-high pressured, in an orthorhombic unit cell $\approx 2\sqrt{2}a_p \times 2\sqrt{2}a_p \times a_p$, where the lattice constant a decreases and c increases with increasing oxygen content, but variations with strontium concentration are small. The most homogeneous phases were obtained with $x = 0.775$

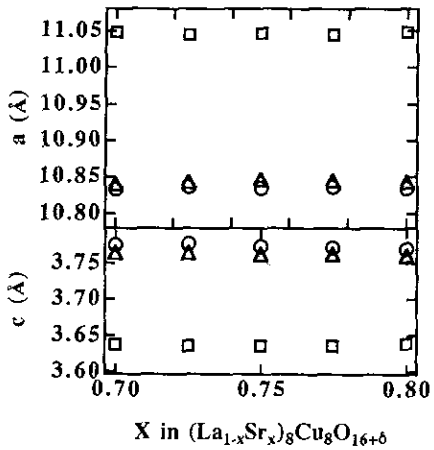

FIG. 4. Strontium-concentration dependence of lattice constants a and c of $(La_{1-x}Sr_x)_8Cu_8O_{16+\delta}$: Ar-annealed (squares), O_2-annealed (triangles), and O_2-high pressure (circles).

so we used them for refinements. A very small amount of impurities, however, remained and could never be removed, and so some peaks were omitted from the calculations; 29.70°–30.10° and 31.5°–31.8° (1-1-2 phase) for Ar-annealed; 29.60°–29.8°, 31.50°–31.80° and 34.26°–34.60° (1-1-2 phase), 31.80°–32.40° (3-2-6 phase) for O_2-annealed; 30.40°–31.60° (14-24-41 phase) and 31.80°–32.40° (3-2-6 phase) for O_2-high pressure. No other peaks which can be assigned to a superstructure, the ordering of La and Sr for example, were observed. The systematic absence of reflections found already in the electron diffraction patterns (11, 12), $h = 2n + 1$ for $h00$ and $h0l$, was also observed for all three samples using XRD, suggesting three possible space groups; $P4/mbm$, $P\bar{4}b2$, and $P4bm$, corresponding to Fu's choice rather than Fujishita's. To minimize the number of parameters, the most symmetric space group $P4/mbm$ was chosen at the beginning. Calculations were started with a fixed overall isotropic thermal parameter of 1 Å^2, and the positions of different atoms were placed as in the ideal cubic perovskite structure without oxygen vacancies in the same way of the literature, which is shown in Table 1.

$(La_{0.225}Sr_{0.775})_8Cu_8O_{16.07}$ (8-8-16.07). After refinement of the background, peak-profile and cell parameters and the scale factor with fixed atomic parameters R_i (integrated intensity R-factor) was reduced to 0.3861, which implies the correctness of the perovskite model. Then refinement of the La(Sr) and Cu positions reduced it to 0.1858. During subsequent refinement of the occupancies of oxygen positions, those of O(1), O(2), and O(5) were found to be low and these oxygen atoms were removed from further calculations (see also Fig. 6). There removals are consistent with the oxygen content, and after final refinement the discrepancy factors were reduced to R_i = 0.0560 (R_e = 0.0300, R_p = 0.0457, and R_{wp} = 0.0637). The refined lattice constants are a = 11.0464(2) Å and c = 3.6390(1) Å, which are in good agreement with those reported using neutron diffraction, and the overall isotropic thermal parameter is 0.18(11) Å^2. Resulting atomic positions are listed in Table 1. Then we tried calculations using the lower symmetric space groups, $P\bar{4}b2$ and $P4bm$. Refinement with $P\bar{4}b2$, that is, with variable z-coordinations of La(Sr) and O(6), lowered the discrepancy factor a little (R_i = 0.0477) and resulted in slight deviations of these atoms in the z-direction from their starting positions (see Table 2). Refinement with variable z-coordinations of other atoms using the space group $P4bm$ gave no significant changes but larger estimated standard deviations of atomic positions, so that the results are not presented here.

$(La_{0.225}Sr_{0.775})_8Cu_8O_{18.14}$ (8-8-18.14). The structure of $(La_{0.225}Sr_{0.775})_8Cu_8O_{18.14}$ was refined in almost the same manner as described above. The occupation factors on O(1) and O(5) positions were found to decrease during the calculation and then these atoms were excluded. The extra oxygen, 0.14 per formula units, is too small to refine and we neglected it. The refinement converged with the parameters, a = 10.8420(2) Å, c = 3.7627(1) Å, B = 0.29(8) Å^2 and R_i = 0.0328 (R_e = 0.0249, R_p = 0.0404, and R_{wp} = 0.0569) and resulting atomic parameters are shown in Table 1. Calculation adopting $P\bar{4}b2$ or $P4bm$ as the space group did not improve the discrepancy factors and gave no meaningful differences.

$(La_{0.225}Sr_{0.775})_8Cu_8O_{18.55}$ (8-8-18.55). In the refinement of the structure of $(La_{0.225}Sr_{0.775})_8Cu_8O_{18.55}$, the occupancy of O(1) was quickly lowered to 0; a residue of 0.25(4) too large to ignore remained on O(5) position. Then we fixed its occupancy at 0.1375 on account of the formula. The finally converged parameters are a = 10.8386(2) Å, c = 3.7705(1) Å, B = 0.33(10) Å^2, and R_i = 0.0416 (R_e = 0.0291, R_p = 0.0456, and R_{wp} = 0.0652) and atomic positions are given in Table 1. Subsequent calculations with the lower symmetry group never changed the atomic parameters significantly, but instead made the discrepancy factors worse. Observed and calculated profiles of the XRD patterns for $(La_{0.225}Sr_{0.775})_8Cu_8O_{18.55}$ in the space group $P4/mbm$ refined above are presented in Fig. 5.

Figure 6 shows schematic relations between the structures of the 8-8-20, 4-4-10, 8-8-18, and 8-8-16 phases. Large open circles and polygons stand for the La(Sr) cations and Cu–O_n polyhedrons respectively; small circles represent oxygen vacancies, shaded circles O(1), open circles O(2), and closed circles O(5). The full insertion of oxygen atoms into these vacancies gives a perovskite composition. Removal of the closed circles results in the 8-8-20 structure, while the 4-4-10 structure can be obtained by omitting dashed circles. The number of oxygen vacancies in these two phases are the same (four

TABLE 1
Refined Atomic Positions of $(La_{0.255}Sr_{0.775})_8Cu_8O_{16+\delta}$ (δ = 0.07, 2.14, and 2.55) in the Space Group *P4/mbm*

	Starting positions				8-8-16.07[a]			8-8-18.14[b]			8-8-18.55[c]		
Atoms	*x*	*y*	*z*	Sites	*x*	*y*	*z*	*x*	*y*	*z*	*x*	*y*	*z*
La(Sr)	0.25	0	0.5	8*j*	0.2397(5)	0.0331(4)	0.5	0.2475(6)	0.0262(3)	0.5	0.2471(7)	0.027(4)	0.5
Cu(1)	0	0	0	2*a*	0	0	0	0	0	0	0	0	0
Cu(2)	0	0.5	0	2*d*	0	0.5	0	0	0.5	0	0	0.5	0
Cu(3)	0.25	0.75	0	4*g*	0.2841(8)	*x* + 0.5	0	0.2714(6)	*x* + 0.5	0	0.2712(8)	*x* + 0.5	0
O(1)	0	0	0.5	2*b*	—	—	—	—	—	—	—	—	—
O(2)	0	0.5	0.5	2*c*	—	—	—	0	0.5	0.5	0	0.5	0.5
O(3)	0.25	0.75	0.5	4*h*	0.313(3)	*x* + 0.5	0.5	0.283(2)	*x* + 0.5	0.5	0.288(3)	*x* + 0.5	0.5
O(4)	0.125	0.625	0	4*g*	0.116(3)	*x* + 0.5	0	0.122(3)	*x* + 0.5	0	0.125(3)	*x* + 0.5	0
O(5)	0.375	0.875	0	4*g*	—	—	—	—	—	—	0.389(28)	*x* + 0.5	0
O(6)	0.125	0.125	0	4*i*	0.104(3)	0.139(3)	0	0.104(3)	0.144(3)	0	0.107(4)	0.139(4)	0

Note. Lattice constants: [a] a = 11.0464(2) Å, c = 3.6390(1) Å, [b] a = 10.8420(1) Å, c = 3.7627(1) Å; [c] a = 10.8386(2) Å, c = 3.7705(1) Å. Discrepancy factors: [a] R_i = 0.0560, R_p = 0.0457, R_{wp} = 0.0637, R_e = 0.0300. [b] R_i = 0.0328, R_p = 0.0404, R_{wp} = 0.0569, R_e = 0.0277. [c] R_i = 0.0416, R_p = 0.0456, R_{wp} = 0.0652, R_e = 0.0291. Overall isotropic thermal parameters: [a] 0.18(11) Å^2, [b] 0.29(8) Å^2, [c] 0.33(10) Å^2.

oxygens per unit cell), but the manner of oxygen-vacancy ordering is different from each other. Removal of the closed and shaded circles gives the structure of the 8-8-18 phase, and another omission of the open circles results in the 8-8-16 structure. In such a manner, the 8-8-20, 8-8-18, and 8-8-16 structures can be obtained by the stepwise removal of oxygen atoms from an ideal perovskite composition. The additional oxygen atoms, however, in the 8-8-18 phase (O_2-high pressure) are placed at the closed circle position O(5), which does not interfere with making the 8-8-20 structure.

Several selected interatomic distances calculated from the atomic positions in Tables 1 and 2 are collected in Table 3. Structural properties of the 8-8-16 and 8-8-18 phase have already discussed by Fu *et al.* and our results with the space group *P4/mbm* are in good agreement with theirs. Calculations for 8-8-16.07 in $P\bar{4}b2$ give the eight different values for La(Sr)–O distances, some of which are degenerate in *P4/mbm*, and make us suggest a more complicated arrangement of oxygen atoms around lanthanum and strontium. The Cu(2)–O(4) distance in 8-8-16.07, 1.82 Å (*P4/mbm*), and 1.86 Å ($P\bar{4}b2$) can be compared with 1.85 Å in Cu_2O and 1.80 Å in $YBa_2Cu_3O_6$ (19) and shows the monovalent character of Cu(2); it is somewhat extended in other oxygenated forms; 1.87 Å (8-8-18.14) and 1.92 Å (8-8-18.55). These increases imply the change

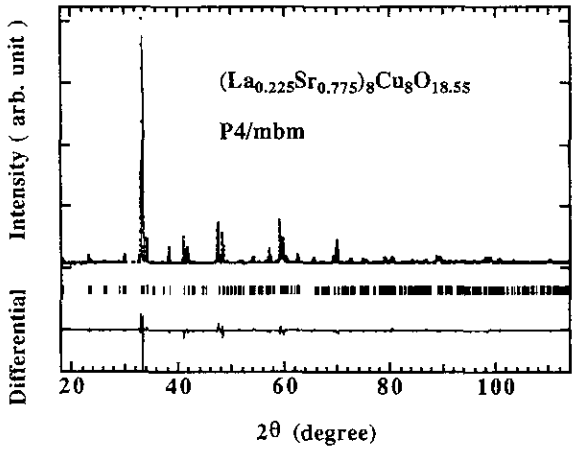

FIG. 5. X-ray Rietveld refinement patterns for $(La_{0.225}Sr_{0.775})_8Cu_8O_{18.55}$ in the space group *P4/mbm* at room temperature. The observed and calculated data are shown by a continuous and dots, respectively. The difference between them is shown in the lower portion. The bars drawn in the middle portion show the positions of the reflection peaks.

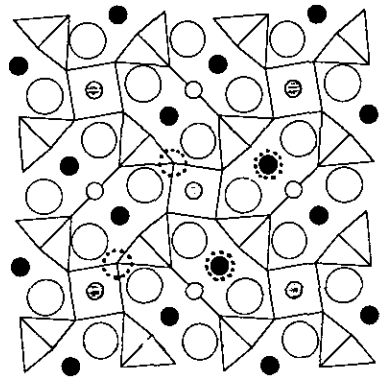

FIG. 6. A schematic projection onto the (001) plane of the structure of the 8-8-16 + δ phases. Large open circles and polygons represent La(Sr) cations and CuO_n polyhedrons. Small shaded, open, and closed circles represent O(1), O(2), and O(5) positions, respectively. These circles stand for oxygen vacancies and the full insertion of the oxygen atoms into these positions gives the perovskite composition. Dotted circles are the oxygen vacancies in the 4-4-10 structure.

TABLE 2
Refined Atomic Positions of $(La_{0.225}Sr_{0.775})_8Cu_8O_{16+\delta}$ ($\delta = 0.07$) in the Space Group P4b2

Atoms	Sites	x	y	z
La(Sr)	8*d*	0.2396(5)	0.033(4)	0.486(3)
Cu(1)	2*a*	0	0	0
Cu(2)	2*c*	0	0.5	0
Cu(3)	4*g*	0.2840(7)	$x + 0.5$	0
O(1)	2*b*	—	—	—
O(2)	2*d*	—	—	
O(3)	4*h*	0.314(3)	$x + 0.5$	0.5
O(4)	4*g*	0.119(3)	$x + 0.5$	0
O(5)	4*g*	—	—	—
O(6)	8*i*	0.106(3)	0.136(3)	0.09(1)

Note. Lattice constants: $a = 11.0464(2)$ Å, $c = 3.6390(1)$ Å. Discrepancy factors: $R_i = 0.0477$, $R_p = 0.0447$, $R_{wp} = 0.0615$, $R_e = 0.0300$. Overall isotropic thermal parameters: 0.09(11) Å^2.

of the copper oxidation state to divalent. The Cu(3)–O(3) distance, which is perpendicular to the x–y plane, increases with increasing oxygen content according to the expansion of the lattice constant c. The decrease of the Cu(3)–O(4) distance, which is trans to oxygen vacancy, with increasing oxygen content; 2.62 Å (8-8-16.07), 2.29 Å (8-8-18.14, −13%), and 2.24 Å (8-8-18.55, −15%), cannot be explained only by the shrinkage of the a-axis (about −2%). Actually the Cu(3)–Cu(6) distance decreases at a rate of the same order (about −4%) from 2.03 Å (8-8-16.07) to 1.94 Å (8-8-18.14) or 1.95 Å (8-8-18.55). The larger decreasing rate (−13% to −15%) of the Cu(3)-O(4) distance is caused by the random occupation by the extra oxygen atoms on O(5) site. The longer distance between the central atom and apical oxygen in the pyramidal coordination results from unequal electron occupancy of the d_z2 and d_x2-_y2 orbitals (20, 21) and this distortion can be relaxed with the octahedral-like arrangement by additional oxygen. In addition, the similarity of this distance in 8-8-18.14 (2.29 Å) to that in 8-8-18.55 (2.24 Å) in comparison with that in 8-8-16.07 (2.62 Å) makes us presume a considerable oxygen occupancy on the O(5) site in 8-8-18.14, which was neglected in the Rietveld calculation. As a matter of fact, the occupancy of O(5) in the Rietveld refinement of $(La_{0.225}Sr_{0.775})_8Cu_8O_{18.14}$ did not readily decrease, while that of O(1) quickly converged near to 0.

Electrical and Magnetic Properties

Metallic behaviors of air-quenched "$(La_{0.25}Sr_{0.75})_8Cu_8O_{16}$" and air-annealed "$(La_{0.25}Sr_{0.75})_8Cu_8O_{17.6}$" have been already reported by Fu *et al.* (9) and Fujishita *et al.* (15). The slight upturn in the resistivity below 100 K has

TABLE 3
Interatomic Distances in $(La_{0.225}Sr_{0.775})_8Cu_8O_{16+\delta}$ for $\delta = 0.07$, 2.14 and 2.55 (Å)

	8-8-16.07 in *P4/mbm*		8-8-16.07 in $p\bar{4}b2$		8-8-18.14 in *P4/mbm*		8-8-18.55 in *P4/mbm*	
Cu(10–O(6)	1.917(5)[a]	×4	1.931(6)[a]	×4	1.923(6)[a]	×4	1.900(8)[a]	×4
Cu(2)–O(2)	—		—		1.881(1)[a]	×2	1.885(1)[a]	×2
Cu(2)–O(4)	1.817(7)[a]	×2	1.859(7)[a]	×2	1.871(7)[a]	×2	1.920(9)[a]	×2
Cu(2)–O(5)	—		—		—		1.70(6)[c]	×2
Cu(3)–O(3)	1.875(2)[a]	×2	1.877(2)[a]	×2	1.8901(5)[a]	×2	1.902(1)[a]	×2
Cu(3)–O(4)	2.620(7)[a]	×1	2.578(7)	×1	2.290(7)[a]	×1	2.237(9)[a]	×1
Cu(3)–O(5)	—		—		—		1.81(6)[a]	×1
Cu(3)–O(6)	2.025(5)[b]	×2	2.064(6)[g]	×2	1.935(6)[b]	×2	1.949(8)[b]	×2
La(Sr)–O(2)	—		—		2.752(1)[c]	×1	2.756(1)[c]	×1
La(Sr)–O(3)	3.147(5)[c]	×1	3.160(5)	×1	2.808(4)[c]	×1	2.849(4)[c]	×1
La(Sr)–O(3)	2.562(3)[d]	×1	2.554(3)[d]	×1	2.662(3)[d]	×1	2.632(3)[d]	×1
La(Sr)–O(4)	2.586(2)[e]	×2	2.545(2)[e]	×1	2.573(1)[e]	×2	2.569(1)[e]	×2
			2.617(2)[h]	×1				
La(Sr)–O(5)	—		—		—		2.856(1)[d]	×1
La(Sr)–O(6)	2.634(3)[a]	×2	2.365(6)[a]	×1	2.753(3)[a]	×2	2.705(3)[a]	×2
			2.885(5)[i]	×1				
La(Sr)–O(6)	2.613(3)[f]	×2	2.829(6)[j]	×1	2.608(3)[f]	×2	2.656(3)[f]	×2
			2.455(5)[k]	×1				

Note. Symmetry codes for oxygen atoms. [a] x, y, z; [b] $y, 1 - x, z$; [c] $1 - y, x, z$; [d] $x, -1 + y, z$; [e] $1/2 - x, -1/2 + y, z$; [f] $y, -x, z$; [g] $y, 1 - x, -z$; [h] $1/2 - x, -1/2 + y, z + 1$; [i] $x, y, 1 + z$; [j] $y, -x, -z$; [k] $y, -x, 1 - z$.

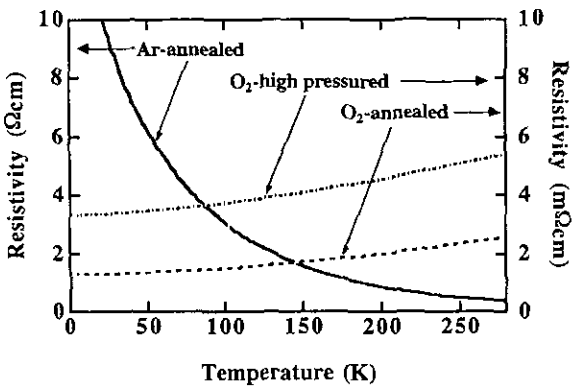

FIG. 7. The temperature dependence of the resistivity ρ of the Ar-annealed (solid line), the O_2-annealed (dashes) and the O_2-high pressure (dashes with dots) samples with $x = 0.775$.

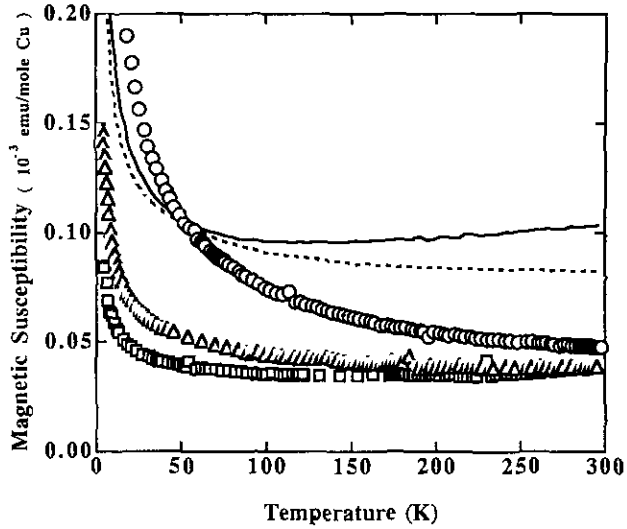

FIG. 9. Temperature dependence of the magnetic susceptibility of $(La_{0.225}Sr_{0.775})_8Cu_8O_{16.07}$ (squares), $(La_{0.225}Sr_{0.775})_8Cu_8O_{18.14}$ (triangles), $(La_{0.225}Sr_{0.775})_8Cu_8O_{18.55}$ (circles), $(La_{0.8571}Sr_{0.1429})_4Cu_4O_{10}$ (solid line) and $(La_{0.8333}Sr_{0.1666})_5Cu_5O_{13}$ (dashes).

been also reported for air-quenched sample. Aside from the measurements of the O_2-annealed samples, these observations on air-quenched samples are unreliable because of their inhomogeneity as described above.

Figure 7 shows the temperature dependence of resistivity ρ of the 8-8-16 phase; $x = 0.775$. At first glance, this phase is not metallic but shows semiconductor-like behavior. The reported upturn is substantial and results from this property of the 8-8-16 phase, and the increase in the reported resistivity at higher temperature shows vividly the contamination by the oxygenated phase (8-8-18) in their samples. Fitting the resistivity profiles of the 8-8-16 phase ($x = 0.7$–0.8, data not shown) to the equation $\ln \rho = C_1T^{-1} + C_2$ (C_1 and C_2 are fitting parameters) is not successful throughout the temperature range of the measurement, but the fit between observed and calculated profiles using lowest-temperature data (<20 K) is good and gives decreasing C_1's with increasing strontium concentration (see Fig. 8). C_1 is related to the activation energy (ΔE) for semiconductors by $\Delta E = C_1k_B/e$.

Figure 7 also shows temperature dependence of the resistivity of the 8-8-18 phase ($x = 0.7775$, O_2-annealed and O_2-high pressure). Both compositions exhibit metallic behavior. The resistivity tended to increase with increasing x (data not shown), but we cannot estimate their x dependence because the sinterability is different from sample by sample. In addition, the O_2-high-pressured sample with $x = 0.80$ showed a somewhat strange curve: a linear decrease with increasing temperature (data not shown), which we also cannot explain, but we consider that a somewhat large oxygen content (18.60) and a largely deviant copper valence (2.45, see Phase Relations and Oxygen Contents) have something to do with it.

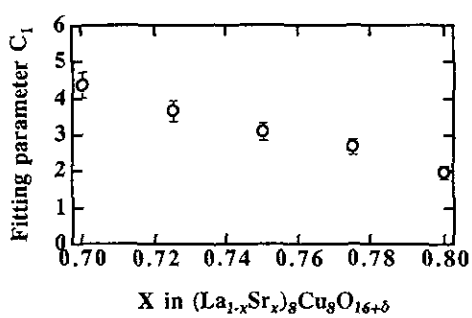

FIG. 8. Fitting parameter C_1 for the resistivity ρ (<20 K) of the Ar-annealed samples with the equation $\ln \rho = C_1T^{-1} + C_2$, vs the stontium concentration ($0.70 \leq x \leq 0.80$). $C_1 \times k_B/e$ (k_B, Boltzmann constant; e, charge of an electron) is related to the energy gap for semiconductors.

The magnetic susceptibility vs temperature curve for the 8-8-16 ($x = 0.775$) is shown in Fig. 9. The data for the other compounds, the 4-4-10 ($x = 0.1429$) and the 5-5-13 ($x = 0.1666$), which have been recently reported by us, are also presented in the same figure. Each shows a slight temperature dependence above 100 K and an abrupt upturn in the lowest temperature range. These characteristics of the profiles may result from a large part showing Pauli paramagnetism contaminated by a small amount showing Curie–Weiss behavior. Then we tried to fit the observed profiles with the function

$$\chi(T) = C/(T + \theta) + \chi_0 + \chi_1T.$$

The first term shows the Curie–Weiss law and χ_0 gives other temperature-independent parts; χ_1 was added to reflect the small temperature-dependence. The converged fitting parameters are collected in Table 4. The Curie constant C is proportional to the number of spins, and is

TABLE 4
Magnetic Susceptibility Data

Compounds	C (emu · K/mole)	θ (K)	χ_0 (emu/mole)	χ_1 (emu/K · mole)
$(La_{0.225}Sr_{0.775})_8Cu_8O_{16.07}$	0.397×10^{-3}	3.02	0.030×10^{-3}	0.19×10^{-7}
$(La_{0.225}Sr_{0.775})_8Cu_8O_{18.14}$	0.701×10^{-3}	2.25	0.039×10^{-3}	-0.14×10^{-7}
$(La_{0.225}Sr_{0.775})_8Cu_8O_{18.55}$	4.070×10^{-3}	8.10	0.038×10^{-3}	-0.15×10^{-7}
$(La_{0.8571}Sr_{0.1429})_4Cu_4O_{10}$	1.583×10^{-3}	4.16	0.073×10^{-3}	0.87×10^{-7}
$(La_{0.8333}Sr_{0.1666})_5Cu_5O_{13}$	0.913×10^{-3}	1.07	0.085×10^{-3}	-0.24×10^{-7}

calculated to be 0.375 for 6.02×10^{23} of spin—1/2 moments with a g-factor of 2. All the calculated Curie-parts are less than 0.5%, so that the upturn (<50 K) can be due to this negligible paramagnetic impurity.

The relatively low values of the temperature independent χ_0 term of the 8-8-16 and 8-8-18 phases (0.030–0.039 $\times 10^{-3}$ emu/mole) compared to those of the 4-4-10 and 5-5-13 phases (0.073–0.085 $\times 10^{-3}$ emu/mole) indicate a decrease in the state density at Fermi energy in these Sr-rich compounds, since the Pauli paramagnetic term is proportional to it.

4. CONCLUSION

$(La_{1-x}Sr_x)_8Cu_8O_{16+\delta}$ can be synthesized for $x = 0.70$ to 0.80 at 1050°C in air. This is the high-temperature phase over the triphasic region of the $(La_{1-x}Sr_x)_3Cu_2O_6$, $SrCuO_2$, and $(La_{1-x}Sr_x)_{14}Cu_{24}O_{41}$ phases, so that quenching as quickly as possible from 1050°C is needed in order to obtain the homogeneous phase. Two distinct phases are isolated: the oxygen-poor 8-8-16 phase and the oxygen rich 8-8-18 phase. As-prepared samples are the mixture of these two phases and it is necessary to anneal it under Ar at 810°C in order to obtain the pure 8-8-16 phase. The 8-8-18 phase shows oxygen nonstoichiometry around $\sigma = 2.05$–2.10 and, by oxygen high-pressure treatment, additional oxygen atoms are inserted into interstitial sites in the basal Cu–O plane rather than into apical positions.

The 8-8-16 phase shows semiconductor-like behavior, while the 8-8-18 phase exhibits metallic resistivity. The magnetic susceptibility data show the Pauli-paramagnetic nature of these phases.

We are now investigating the monophasic oxygen content of these two phases using *in situ* XRD observation at high temperature.

ACKNOWLEDGMENTS

The authors are grateful to Dr. A. Hayashi for help. This work was partly supported by a Grant-in-Aid for Scientific Research on Priority Areas, "Science of High T_c Superconductivity" given by the Ministry of Education, Science and Culture of Japan.

REFERENCES

1. J. B. Torrance, Y. Tokura, A. I. Nazzal, A. Bezinge, T. C. Huang, and S. S. P. Parkin, *Phys. Rev. Lett.* **61,** 1127 (1988), and references therein.
2. M. Takano, M. Azuma, Z. Hiroi, Y. Bando, and Y. Takeda, *Physica C* **176,** 441 (1991).
3. M. Azuma, Z. Hiroi, M. Takano, Y. Bando, and Y. Takeda, *Nature* **356,** 775 (1992).
4. D. M. De Leeuw, C. A. H. A. Mutsaers, G. P. J. Geelen, and C. Langereis, *J. Solid State Chem.* **80,** 276 (1989).
5. T. Fujita and Y. Maeno, *Jpn. J. Appl. Phys. Part 1,* 34 (1988).
6. CHR. L. Teske and M. Muller-Buschbaum, *Z. Anorg. Allg. Chem.* **379,** 234 (1970).
7. N. Nguyen, L. Er-Rakho, C. Michel, J. Choisnet, and B. Raveau, *Mater. Res. Bull.* **15,** 891 (1980).
8. L. Er-Rakho, C. Michel, and B. Raveau, *J. Solid State Chem.* **73,** 514 (1988).
9. W. T. Fu, Q. Xu, A. A. Verheijen, J. M. von Ruitenbeek, H. W. Zandbergen, and L. J. de Jongh, *Solid State Commum.* **73,** 291 (1990).
10. N. Nguyen, J. Choisnet and B. Raveau, *Mater. Res. Bull.* **17,** 567 (1982).
11. W. T. Fu, F. C. Mijlhoff, D. J. W. Ijdo, and V. Ponec, *Solid State. Commun.* **83,** 59 (1992).
12. W. T. Fu, D. J. W. Ijdo, and R. B. Helmholdt, *Mater. Res. Bull.* **27,** 287 (1992).
13. K. Otzschi, A. Hayashi, Y. Fujiwara, and Y. Ueda, *J. Solid State Chem.* **105,** 573 (1993).
14. K. Otzschi and Y. Ueda, *J. Solid State Chem.* **107,** 149 (1993).
15. H. Fujishita, M. Sera, and M. Sato, *Physica C* **175,** 165 (1991).
16. F. Izumi, *J. Crystallogr. Soc. Jpn.* **27,** 23 (1985).
17. E. M. McCarron, III, M. A. Subramanian, J. C. Calabrese, and R. L. Harlow, *Mater. Res. Bull.* **23,** 1355 (1988).
18. T. Siegrist, L. F. Schneemeyer, S. A. Sunshine, and J. V. Wszczak, *Mater. Res. Bull.* **23,** 14295 (1988).
19. P. Bordet, C. Chaillout, J. J. Capponi, J. Chenavas, and M. Marezio, *Nature* **327,** 687 (1987).
20. C. Michel, L. Er-Rakho, M. Hervieu, J. Pannetier, and B. Raveau, *J. Solid State Chem.* **68,** 143 (1987).
21. K. R. Poeppelmeier, M. E. Leonowicz, and J. M. Longo, *J. Solid State Chem.* **44,** 89 (1982).